Synthesis and Solid-state Structure of $[Pd_6Ru_6(CO)_{24}]^{2-}$ Electrochemistry and ^{13}C Nuclear Magnetic Resonance Spectra of $[Fe_6Pd_6H(CO)_{24}]^{3-}$ and $[Pd_6Ru_6(CO)_{24}]^{2-}$ †

Elisa Brivio,[a] Alessandro Ceriotti,[a] Roberto Della Pergola,*[,a] Luigi Garlaschelli,[a] Francesco Demartin,[b] Mario Manassero,*[,b] Mirella Sansoni,[b] Piero Zanello,*[,c] Franco Laschi[c] and Brian T. Heaton*[,d]

[a] *Dipartimento di Chimica Inorganica, Metallorganica e Analitica and Centro del CNR, University of Milano, via G. Venezian 21, 20133 Milano, Italy*

[b] *Istituto di Chimica Strutturistica Inorganica, University of Milano, via G. Venezian 21, 20133 Milano, Italy*

[c] *Dipartimento di Chimica dell' Università, Pian dei Mantellini 44, 53100 Siena, Italy*

[d] *Chemistry Department, University of Liverpool, Liverpool L69 3BX, UK*

The cluster $[Pd_6Ru_6(CO)_{24}]^{2-}$ was obtained in good yield from the reaction of $[Ru_3H(CO)_{11}]^-$ with $[Pd(NCPh)_2Cl_2]$. The salt $[NEt_4]_2[Pd_6Ru_6(CO)_{24}]$ crystallized in the triclinic space group $P\bar{1}$ (no. 2) with $a = 11.514(5)$, $b = 11.602(5)$, $c = 11.933(5)$ Å, $\alpha = 73.01(3)$, $\beta = 78.25(3)$, $\gamma = 65.26(4)°$, $Z = 1$. Data were collected at room temperature, giving 5968 unique reflections. The structure was solved by direct methods. The final discrepancy indices were $R = 0.024$ and $R' = 0.026$ for 4129 independent reflections with $I > 3\sigma(I)$. The metal skeleton consists of a trigonally distorted octahedron of palladium atoms, capped by six ruthenium atoms with twelve terminal, six edge- and six face-bridging carbonyl ligands. This ruthenium–palladium cluster adopts the same metallic polyhedron as $[Fe_6Pd_6H(CO)_{24}]^{3-}$ but possesses two valence electrons less. The solution ^{13}C NMR spectra of both anions are in agreement with the solid-state structures and electrochemical analysis shows that they produce labile congeners: $[Pd_6Ru_6(CO)_{24}]^{2-}$ undergoes a one-electron oxidation with formation of the relatively stable monoanion; $[Fe_6Pd_6H(CO)_{24}]^{3-}$ can be oxidized and reduced, to give corresponding anions with charges of 2− to 5−.

The molecular structures of heterometallic clusters are frequently unpredictable because of the different steric and electronic requirements of the different metals,[1] which obviously affect their ability to lose/accept electrons.[2] Since ruthenium clusters require a large number of terminal carbonyl ligands,[3] whereas palladium clusters possess only bridging carbonyl ligands,[4] it was considered worthwhile to investigate the ruthenium–palladium mixed-metal system, irregular metal polyhedra with well defined different co-ordination sites for the two elements being expected.

The reaction of $[Ru_3H(CO)_{11}]^-$ with palladium(II) salts yielded the dianion $[Pd_6Ru_6(CO)_{24}]^{2-}$ **1**, which was isolated as the $[NEt_4]^+$ salt. The metal framework of the cluster possesses six semi-interstitial palladium atoms, connected to bridging ligands only and six capping ruthenium atoms linked to both terminal and bridging carbonyl groups. The complex is isostructural with $[Fe_6Pd_6H(CO)_{24}]^{3-}$ **2**,[5] but it has two less cluster valence electrons. In order to rationalize this difference, ^{13}C NMR spectra and electrochemical measurements have been carried out on both the ruthenium- and iron–palladium clusters, as part of a comparative investigation.

Results and Discussion

Synthesis of $[Pd_6Ru_6(CO)_{24}]^{2-}$.—Oxidative condensations between anionic iron carbonyl species and halide complexes of Pt^{II} or Pd^{II} have been successfully used for the syntheses of mixed-metal platinum–[6] and palladium–iron[5] clusters. For the preliminary investigations on the ruthenium–palladium system, an analogous synthetic approach using $[Ru_3H(CO)_{11}]^-$ and $[Pd(NCPh)_2Cl_2]$ was chosen. These reagents, in the molar ratio 1 : 1.2, in acetone at −78 °C, condense smoothly on allowing the solution to warm to room temperature, resulting in the formation of the new anion $[Pd_6Ru_6(CO)_{24}]^{2-}$. Using these conditions the reaction is reproducible and the product can easily be recovered after extraction of neutral by-products which are very soluble in aromatic solvents. Unfortunately, low yields (15–20%) were always obtained, owing to incomplete reaction and formation of palladium metal. Any change in the synthetic procedure involving the ratio between the reagents, the nature of the starting palladium complex, the sequence of addition of reactants, or the counter ion did not result in any appreciable improvement. Better results were obtained by a slight modification of the above procedure, employing crude $Na[Ru_3H(CO)_{11}]$ in MeOH: in this case the yields increased to about 60% (see Experimental section).

All salts of the cluster are soluble in acetone or acetonitrile and slightly less soluble in tetrahydrofuran (thf). The values of ν(CO), in the IR spectrum of the $[NEt_4]^+$ salt, in thf solution are 2018vs, 2005(sh), 1957m, 1860m and 1822m cm^{-1}. The ^1H NMR measurements provide no evidence for resonances which could be attributable to hydride species, confirming the formulation of the compound.

The cluster does not react with CO at atmospheric pressure; any attempt to reduce the anion with chemical reagents brought about extensive decomposition. On the contrary, oxidation with $[Fe(C_5H_5)_2]PF_6$ resulted in the formation of a single product

† *Supplementary data available:* see Instructions for Authors, *J. Chem. Soc., Dalton Trans.*, 1994, Issue 1, pp. xxiii–xxviii.

Non-SI unit employed: G = 10^{-4} T.

Table 1 Atomic coordinates with estimated standard deviations in parentheses for $[NEt_4]_2[Pd_6Ru_6(CO)_{24}]$

Atom	x	y	z	Atom	x	y	z
Pd(1)	0.423 71(3)	0.130 09(3)	−0.148 97(3)	C(3)	0.439 1(4)	0.310 4(4)	−0.132 6(4)
Pd(2)	0.670 42(3)	−0.050 36(3)	−0.110 50(3)	C(4)	0.253 3(4)	0.191 1(5)	−0.225 7(4)
Pd(3)	0.563 35(3)	0.153 73(3)	0.003 57(3)	C(5)	0.811 4(4)	−0.230 5(4)	−0.134 6(4)
Ru(4)	0.517 14(3)	−0.097 66(3)	−0.232 59(3)	C(6)	0.559 5(4)	0.229 3(4)	0.146 2(4)
Ru(5)	0.780 87(3)	−0.063 47(4)	0.082 23(3)	C(7)	0.413 5(5)	−0.032 6(5)	−0.356 4(4)
Ru(6)	0.299 67(4)	0.297 79(4)	0.002 66(3)	C(8)	0.651 4(4)	−0.206 5(4)	−0.318 8(4)
O(1)	0.626 3(3)	0.116 7(3)	−0.354 8(3)	C(9)	0.946 1(5)	−0.175 6(5)	0.038 8(4)
O(2)	0.804 2(3)	0.138 4(3)	−0.149 5(3)	C(10)	0.848 5(4)	0.008 6(5)	0.161 2(4)
O(3)	0.479 3(3)	0.374 5(3)	−0.211 1(3)	C(11)	0.296 9(5)	0.433 5(5)	0.060 1(5)
O(4)	0.229 2(3)	0.267 0(3)	−0.314 7(3)	C(12)	0.159 9(5)	0.410 1(5)	−0.083 2(4)
O(5)	0.898 7(3)	−0.239 5(3)	−0.204 1(3)	N	−0.165 8(3)	0.342 5(3)	−0.482 5(3)
O(6)	0.596 7(3)	0.308 7(3)	0.140 3(3)	C(111)	−0.163 4(5)	0.379 0(5)	−0.615 0(5)
O(7)	0.351 6(4)	0.001 4(4)	−0.431 9(3)	C(112)	−0.228 1(6)	0.317 6(6)	−0.665 7(5)
O(8)	0.731 6(4)	−0.271 7(3)	−0.372 5(3)	C(121)	−0.092 6(4)	0.409 1(5)	−0.451 5(5)
O(9)	1.047 0(4)	−0.244 0(4)	0.012 6(4)	C(122)	−0.086 4(5)	0.386 5(6)	−0.322 6(5)
O(10)	0.892 2(3)	0.049 4(4)	0.210 4(3)	C(131)	−0.300 8(4)	0.381 7(5)	−0.423 4(5)
O(11)	0.297 5(4)	0.515 4(4)	0.093 1(4)	C(132)	−0.378 2(5)	0.529 1(5)	−0.455 6(6)
O(12)	0.072 6(4)	0.479 5(4)	−0.133 6(4)	C(141)	−0.102 0(5)	0.194 7(5)	−0.438 6(5)
C(1)	0.584 2(4)	0.051 5(4)	−0.279 9(4)	C(142)	0.036 8(5)	0.135 7(5)	−0.487 3(5)
C(2)	0.762 3(4)	0.072 8(4)	−0.074 4(4)				

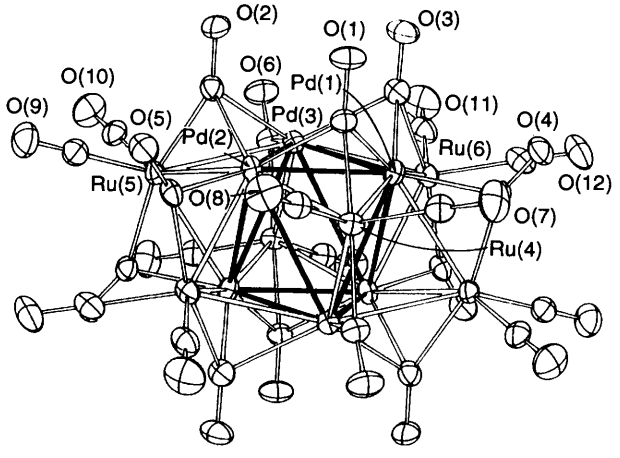

Fig. 1 The ORTEP drawing for the anion $[Pd_6Ru_6(CO)_{24}]^{2-}$. Thermal ellipsoids are drawn at the 30% probability level

which was tentatively formulated as $[Pd_6Ru_6(CO)_{24}]^-$ on the basis of the IR spectrum [ν(CO) at 2041vs, 2025 (sh), 1982m, 1880m and 1822m cm^{-1} in thf solution] and by analogy with electrochemical results, see below.

Crystal Structure of $[NEt_4]_2[Pd_6Ru_6(CO)_{24}]$.—The crystal structure of $[NEt_4]_2[Pd_6Ru_6(CO)_{24}]$ consists of discrete $[NEt_4]^+$ cations and $[Pd_6Ru_6(CO)_{24}]^{2-}$ anions with interionic contacts not shorter than the sum of the van der Waals radii [shortest contact H(112C)···H(132A) 2.37 Å]. The atomic coordinates of $[NEt_4]_2[Pd_6Ru_6(CO)_{24}]$ are reported in Table 1. An ORTEP[7] view of the whole anion, which possesses crystallographic $\bar{1}(C_i)$ symmetry, and the atom labelling scheme are shown in Fig. 1; selected bond distances and angles are given in Table 2.

The metallic framework of $[Pd_6Ru_6(CO)_{24}]^{2-}$ can be described as a trigonally elongated octahedron of palladium atoms; the six faces along the three-fold axis are capped by six ruthenium atoms. The resulting skeleton, possessing idealized $\bar{3}m$ (D_{3d}) symmetry, can also be envisaged as being formed by two staggered triangular layers of frequency two (v_2).[8] All ruthenium atoms are connected to two terminal, one edge- and one face-bridging ligand; each palladium atom is linked to one μ-CO, on interlayer ruthenium–palladium edges, and two μ_3-CO, above in-layer Pd_2Ru faces; thus, the whole anion ideally belongs to the D_{3d} point group, as for the metallic framework. Consistent with this description, the metal–metal edges can be grouped into (*a*) in-layer Pd–Pd [average 2.782, range 2.767(2)–2.798(1) Å], (*b*) interlayer Pd–Pd [average 3.180, range 3.068(1)–3.274(2) Å, the large width of this range is

Table 2 Bond distances (Å) and angles (°) within the anion $[Pd_6Ru_6(CO)_{24}]^{2-}$

Pd(1)–Pd(2)	2.767(2)	Pd(1)–Pd(2′)	3.068(1)
Pd(1)–Pd(3)	2.798(1)	Pd(1)–Pd(3′)	3.199(2)
Pd(1)–Ru(4)	2.803(1)	Pd(1)–Ru(5′)	2.680(1)
Pd(1)–Ru(6)	2.789(1)	Pd(2)–Pd(3)	2.781(1)
Pd(2)–Pd(3′)	3.274(2)	Pd(2)–Ru(4)	2.804(1)
Pd(2)–Ru(5)	2.785(1)	Pd(2)–Ru(6′)	2.685(1)
Pd(3)–Ru(4′)	2.680(1)	Pd(3)–Ru(5)	2.792(2)
Pd(3)–Ru(6)	2.787(2)	Pd(1)–C(3)	2.238(6)
Pd(1)–C(1)	2.221(5)	Pd(2)–C(1)	2.216(5)
Pd(1)–C(4)	2.093(5)	Pd(2)–C(5)	2.099(4)
Pd(2)–C(2)	2.271(6)	Pd(3)–C(3)	2.244(5)
Pd(3)–C(2)	2.200(5)	Ru(4)–C(1)	2.069(5)
Pd(3)–C(6)	2.116(6)	Ru(4)–C(7)	1.868(5)
Ru(4′)–C(6)	2.002(5)	Ru(5)–C(2)	2.048(5)
Ru(4)–C(8)	1.876(6)	Ru(5)–C(9)	1.871(6)
Ru(5′)–C(4)	2.003(5)	Ru(6)–C(3)	2.052(5)
Ru(5)–C(10)	1.871(7)	Ru(6)–C(11)	1.878(7)
Ru(6′)–C(5)	2.005(5)	Ru(6)–C(12)	1.864(6)
C(1)–O(1)	1.158(6)	C(2)–O(2)	1.161(6)
C(3)–O(3)	1.161(6)	C(4)–O(4)	1.161(5)
C(5)–O(5)	1.154(5)	C(6)–O(6)	1.149(7)
C(7)–O(7)	1.138(7)	C(8)–O(8)	1.137(6)
C(9)–O(9)	1.141(6)	C(10)–O(10)	1.141(8)
C(11)–O(11)	1.134(9)	C(12)–O(12)	1.143(6)
Pd(1)–C(1)–Pd(2)	77.1(2)	Pd(1)–C(1)–Ru(4)	81.5(2)
Pd(2)–C(1)–Ru(4)	81.7(2)	Pd(2)–C(2)–Pd(3)	76.9(2)
Pd(2)–C(2)–Ru(5)	80.1(2)	Pd(3)–C(2)–Ru(5)	82.1(2)
Pd(1)–C(3)–Pd(3)	77.2(2)	Pd(1)–C(3)–Ru(6)	81.0(2)
Pd(3)–C(3)–Ru(6)	80.8(2)	Pd(1)–C(4)–Ru(5′)	81.7(2)
Pd(2)–C(5)–Ru(6′)	81.7(2)	Pd(3)–C(6)–Ru(4′)	81.2(2)
Pd(1)–C(1)–O(1)	123.1(4)	Pd(2)–C(1)–O(1)	122.3(4)
Ru(4)–C(1)–O(1)	147.0(4)	Pd(2)–C(2)–O(2)	122.3(4)
Pd(3)–C(2)–O(2)	120.5(4)	Ru(5)–C(2)–O(2)	149.7(5)
Pd(1)–C(3)–O(3)	121.8(4)	Pd(3)–C(3)–O(3)	122.2(4)
Ru(6)–C(3)–O(3)	149.0(4)	Pd(1)–C(4)–O(4)	123.9(5)
Ru(5′)–C(4)–O(4)	154.4(5)	Pd(2)–C(5)–O(5)	123.1(4)
Ru(6′)–C(5)–O(5)	155.3(4)	Pd(3)–C(6)–O(6)	125.1(4)
Ru(4′)–C(6)–O(6)	153.7(4)	Ru(4)–C(7)–O(7)	176.9(5)
Ru(4)–C(8)–O(8)	179.0(5)	Ru(5)–C(9)–O(9)	179.8(5)
Ru(5)–C(10)–O(10)	178.2(5)	Ru(6)–C(11)–O(11)	178.5(6)
Ru(6)–C(12)–O(12)	178.5(5)		

Primed atoms are obtained by the symmetry operation $1 - x, -y, -z$.

probably due to packing forces], (*c*) in-layer Pd–Ru [average 2.794, range 2.785(1)–2.804(1) Å] and (*d*) interlayer Pd–Ru [average 2.682, range 2.680(1)–2.685(1) Å]. Thus, the triangular layers are heavily bent, with an average dihedral angle of 13.41° between the Pd_3 and the Pd_2Ru units. Average M–CO bond lengths are Pd–μ_3-C 2.232, Pd–μ-C 2.103, Ru–μ_3-C 2.056, Ru–μ-C 2.003, Ru–C 1.871, μ_3-C–O 1.160, μ-C–O 1.155 and C–O 1.139 Å.

The related cluster $[Fe_6Pd_6H(CO)_{24}]^{3-}$ **2** contains a similar metal polyhedron and an identical ligand disposition. The most striking difference was found in the trigonal elongation of the Pd_6 moiety, which in the iron–palladium cluster is less marked (average in-layer Pd–Pd 2.810 Å and interlayer Pd–Pd 2.948 Å). Direct comparisons of bond distances for the ligands are misleading, because in $[Fe_6Pd_6H(CO)_{24}]^{3-}$ the carbonyls were refined isotropically. However, in keeping with the reduced ionic charge, and consequent smaller back donation, the average C–O distances are longer in **2** (μ_3-C–O 1.19, μ-C–O 1.19 and C–O 1.17 Å).

The two clusters are not isoelectronic: $[Pd_6Ru_6(CO)_{24}]^{2-}$ (158 cluster valence electrons) possesses two electrons less than $[Fe_6Pd_6H(CO)_{24}]^{3-}$. The number of cluster valence electrons found in **1** is exactly that predicted by the polyhedral skeletal electron-pair theory,[9] for a hexacapped octahedron [86 + (6 × 12) = 158]. Thus, it can be suggested that the shortage of electrons weakens the interlayer Pd–Pd bonds. In order to ascertain whether the cluster framework can incorporate different numbers of electrons, and possibly relate the redox changes with structural deformations, the dianion was submitted to electrochemical investigations.

Electrochemistry of $[Pd_6Ru_6(CO)_{24}]^{2-}$.—The cyclic voltammograms in Fig. 2 show the redox aptitude of the dianion $[Pd_6Ru_6(CO)_{24}]^{2-}$ in acetone solution. As far as the first oxidation process and the first reduction process are concerned [Fig. 2(*a*)], the peak height of the cathodic step is almost twice that of the anodic one. Controlled-potential coulometry corresponding to the oxidation process (E_w = +0.5 V) involves one electron per molecule. Analysis[10] of the cyclic voltammetric responses of this one-electron oxidation with scan rate varying from 0.02 to 2.00 V s^{-1} shows that: (*i*) the cathodic-to-anodic peak-current ratio is constant and equal to 1 : 1; (*ii*) the peak-to-peak separation progressively increases from 62 mV at 0.02 V s^{-1} to 89 mV at 2.00 V s^{-1}; (*iii*) the current function $i_{pa}/v^{\frac{1}{2}}$ remains constant. All these data, which are diagnostic of either a chemically or electrochemically reversible one-electron transfer, suggest that no significant structural reorganization occurs upon one-electron removal.[11] Indeed, on carrying out an exhaustive one-electron oxidation of $[Pd_6Ru_6(CO)_{24}]^{2-}$ in acetone solution, the expected cyclic voltammetric response complementary to that of the dianion is not observed due to decomposition of the monoanion $[Pd_6Ru_6(CO)_{24}]^{-}$ as a result of the long electrolysis times. Nevertheless, in tetrahydrofuran solution the electrogenerated monoanion is quite stable.

Analysis of the $[Pd_6Ru_6(CO)_{24}]^{2-/4-}$ reduction step in acetone solution indicates that rather complex electrode mechanisms are operative. Thus: (*i*) the anodic-to-cathodic peak-current ratio, which is 0.78 : 1 at 0.02 V s^{-1}, progressively decreases with scan rate up to the value of 0.31 : 1 at 10.24 V s^{-1}; (*ii*) the peak-to-peak separation progressively increases from 76 mV at 0.02 V s^{-1} to 140 mV at 2.00 V s^{-1}; (*iii*) the current function $i_{pc}/v^{\frac{1}{2}}$ remains substantially constant. All these data are diagnostic of a quasi-reversible two-electron transfer followed by a reversible chemical reaction, which in turn is coupled to slow chemical reactions.

As shown in Fig. 2(*b*), a second one-electron oxidation as well as a second reduction process, apparently involving two closely spaced one-electron additions, can be detected. Both redox changes display directly associated responses in the reverse scan only at high scan rates, thus testifying to the short lifetimes of the electrogenerated congeners. The electrode potentials of the most significant redox changes exhibited by $[Pd_6Ru_6(CO)_{24}]^{2-}$ are summarized in Table 3.

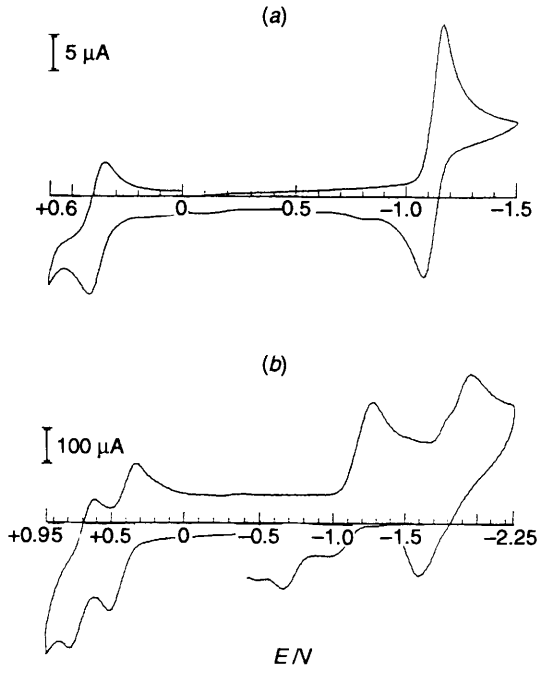

Fig. 2 Cyclic voltammograms recorded at a platinum electrode for $[Pd_6Ru_6(CO)_{24}]^{2-}$ (1.3×10^{-3} mol dm^{-3}) in acetone solution containing $[NBu_4][ClO_4]$ (0.2 mol dm^{-3}). Scan rates: (*a*) 0.05, (*b*) 20.40 V s^{-1}

Table 3 Electrochemical characteristics of the redox changes exhibited by $[Pd_6Ru_6(CO)_{24}]^{2-}$

	Solvent[a]			
	Me_2CO		thf	
Couple	$E^{o\prime}$/V	ΔE_p/mV	$E^{o\prime}$/V	ΔE_p/mV
$[Pd_6Ru_6]^{0/-}$	+0.65[b]	100[b,c]	+0.73[b]	130[b,c]
$[Pd_6Ru_6]^{-/2-}$	+0.41[d]	64[d,e]	+0.35[d]	100[d]
$[Pd_6Ru_6]^{2-/4-}$	−1.09[d]	92[d,f]	−1.16[d]	102[d,f]
$[Pd_6Ru_6]^{4-/5-/6-}$	−1.77[b,f]	270[b,c,g]		

[a] Potential values *vs.* SCE. [b] Measured at 5.12 V s^{-1}. [c] Coupled to fast chemical reactions. [d] Measured at 0.1 V s^{-1}. [e] Coupled to slow chemical reactions. [f] Averaged value between the redox potentials of two almost overlapping reductions. [g] Separation between most cathodic peak and most anodic peak.

The EPR spectrum of $[Pd_6Ru_6(CO)_{24}]^{-}$. At liquid-nitrogen temperature (100 K) the electrogenerated monoanion $[Pd_6Ru_6(CO)_{24}]^{-}$ (see Experimental section) displays a relatively broad and unresolved X-band EPR signal having metal character. Its paramagnetic parameters are g_{av} = 2.07 ± 0.01 and ΔH = 60 ± 3 G. A sharp collapse of the EPR absorption occurs at temperatures higher than the glassy–fluid transition (165 K). In view of the electrochemically tested stability of the monoanion, it is likely that the disappearance of the EPR signal is due to fast relaxation processes rather than to chemical degradation.

Electrochemistry of $[Fe_6Pd_6H(CO)_{24}]^{3-}$.—The redox behaviour of $[Fe_6Pd_6H(CO)_{24}]^{3-}$ is shown in Fig. 3. It displays one oxidation and two separated reduction processes, which are all reversible. Controlled-potential coulometry corresponding to the first cathodic step (E_w = −0.9 V) consumes one electron per molecule. The resulting solution exhibits a cyclic voltammetric profile quite complementary to that of the original trianion. The subsequent exhaustive one-electron

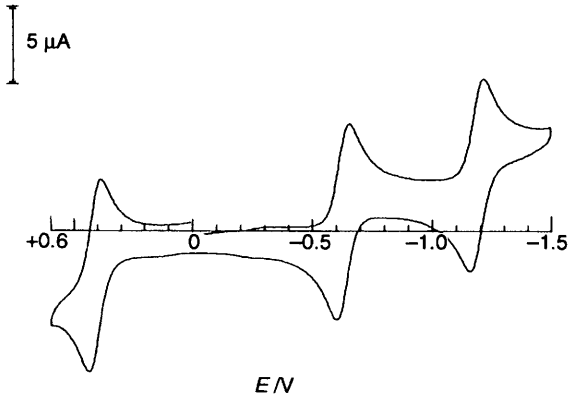

Fig. 3 Cyclic voltammogram recorded at a platinum electrode for $[Fe_6Pd_6H(CO)_{24}]^{3-}$ (1.1×10^{-3} mol dm^{-3}) in acetone solution containing $[NBu_4][ClO_4]$ (0.2 mol dm^{-3}). Scan rate 0.05 V s^{-1}

Table 4 Electrochemical characteristics of the redox changes exhibited by $[Fe_6Pd_6H(CO)_{24}]^{3-}$ in acetone solution

Couple	$E^{o\prime a}$/V	$\Delta E_p{}^b$/mV
$[Pd_6Fe_6]^{2-/3-}$	+0.39	64[c]
$[Pd_6Fe_6]^{3-/4-}$	−0.64	63
$[Pd_6Fe_6]^{4-/5-}$	−1.18[c]	63

[a] Potential values *vs.* SCE. [b] Measured at 0.1 V s^{-1}. [c] Coupled to slow chemical reactions.

reoxidation (E_w = −0.3 V) completely restores the original trianion $[Fe_6Pd_6H(CO)_{24}]^{3-}$, showing that the redox change associated with $[Fe_6Pd_6H(CO)_{24}]^{3-/4-}$ is chemically reversible. Analysis of the cyclic voltammetric response with scan rates varying from 0.02 to 2.00 V s^{-1} shows that: (*i*) the anodic-to-cathodic peak-current ratio is constantly equal to 1:1; (*ii*) the peak-to-peak separation progressively increases from 63 mV at 0.02 V s^{-1} to 74 mV at 2.00 V s^{-1}; (*iii*) the current function $i_{pc}/v^{\frac{1}{2}}$ remains constant. All these data are diagnostic of an electrochemically reversible one-electron transfer. The analyses of the cyclic voltammograms associated with the $[Fe_6Pd_6H(CO)_{24}]^{2-/3-}$ and $[Fe_6Pd_6H(CO)_{24}]^{4-/5-}$ responses afford the same diagnostic results. Thus, the Pd_6Fe_6 core exhibits remarkably flexible redox behaviour and, within the short times of cyclic voltammetry, is able to accommodate both the addition of two electrons and the removal of one electron without significant molecular strain. However, it should be noted that, after a cycle of exhaustive one-electron oxidation (E_w = +0.65 V) followed by exhaustive one-electron reduction, cyclic voltammetry shows that the original trianion $[Fe_6Pd_6H(CO)_{24}]^{3-}$ is recovered in *ca.* 50% yield. This means that a slow chemical decomposition follows the electrogeneration of the dianion $[Fe_6Pd_6H(CO)_{24}]^{2-}$.

The redox potentials of the electron-transfer processes exhibited by $[Fe_6Pd_6H(CO)_{24}]^{3-}$ are reported in Table 4.

The EPR spectra of $[Fe_6Pd_6H(CO)_{24}]^{2-}$ *and* $[Fe_6Pd_6H(CO)_{24}]^{4-}$. In glassy acetone solution, the electrogenerated dianion $[Fe_6Pd_6H(CO)_{24}]^{2-}$ exhibits a complex absorption pattern, which is better interpreted by second-derivative analysis. Three different signals with metallic character can be detected and their relative intensities depend upon the duration of electrolysis. In particular, during the first stage of electrolysis, the low-field signal is the most intense, but this signal slowly decreases with a concomitant increase in the medium- and high-field absorptions as electrolysis proceeds. The relevant X-band EPR parameters are: g_l = 2.086 ± 0.005, ΔH_l = 120 ± 5 G; g_m = 2.045 ± 0.005, ΔH_m = 35 ± 5 G; g_h = 2.009 ± 0.005, ΔH_h = 55 ± 5 G. Increasing the temperature beyond the glassy–fluid transition induces dramatic and irreversible intensity losses of the three absorptions associated with presently

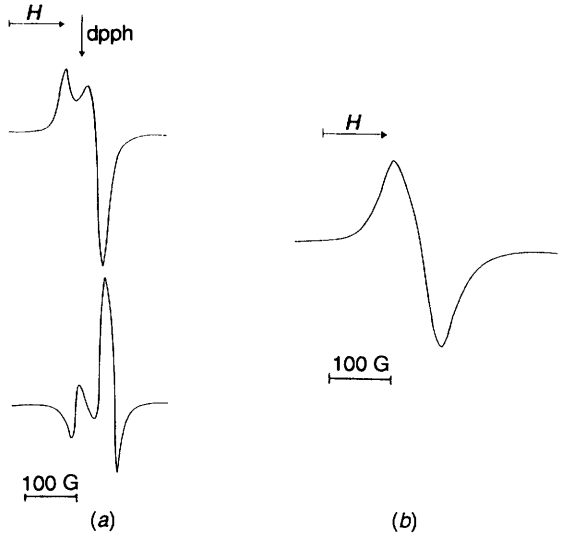

Fig. 4 The EPR spectra of the electrogenerated $[Fe_6Pd_6H(CO)_{24}]^{4-}$ in acetone at (*a*) 100 K (top) with relevant computer simulation (bottom) and (*b*) 160 K

unknown side reactions following the generation of $[Fe_6Pd_6H(CO)_{24}]^{2-}$ and it is likely that the true signal of the dianion is that centred at g = 2.086.

Fig. 4 shows the X-band EPR spectrum of the electrogenerated $[Fe_6Pd_6H(CO)_{24}]^{4-}$ complex, in acetone solution, both at liquid-nitrogen temperature (T = 100 K) (*a*) and in fluid solution (T = 160 K) (*b*). Lineshape analysis of the spectrum at 100 K shows that there is a well resolved axial pattern ($g_{\|} > g_{\perp}$) consistent with the presence of a $S = \frac{1}{2}$ paramagnetic metal-centred system. Computer simulation (SIM14a program)[12] allows an accurate evaluation of the glassy solution spectral parameters: $g_{\|}$ = 2.020 ± 0.005, $g_{\perp}$ = 1.983 ± 0.005 and $\langle g \rangle = \frac{1}{3}(g_{\|} + 2g_{\perp})$ = 1.995 ± 0.005.

The second-derivative analysis provides no evidence for magnetic coupling between the unpaired electron and the hydride hydrogen nucleus of the cluster anion. Such a result is not surprising since the anisotropic spectral linewidths are larger than the corresponding A_{aniso} values; consequently an upper limit for such A_{aniso} parameters can be proposed: $\Delta H_{\|}$(16.5 G) $\geqslant A_{\|}$ and $\Delta H_{\perp}$(19.0 G) $\geqslant A_{\perp}$.

At the glassy–fluid transition (T = 160 K) the axial features evolve to give an unresolved isotropic signal; the relevant parameters (g_{iso} = 1.996 ± 0.005 and ΔH_{iso} = 80 ± 5 G) fit well with those computed at 100 K. The isotropic signal progressively decreases as the temperature increases until it disappears at T = 190 K; this is probably a consequence of the decrease in the paramagnetic relaxation time T_2.[13] Interestingly, refreezing the fluid solution causes quantitative recovery of the starting paramagnetic signal, thus underlining the stability of the tetraanion.

NMR Studies.—$[Pd_6Ru_6(CO)_{24}]^{2-}$. The ^{13}CO NMR spectrum of $[Pd_6Ru_6(CO)_{24}]^{2-}$ (*ca.* 25% ^{13}CO) in acetone solution at 25 °C is entirely in agreement with the solid-state structure; it consists [Fig. 5(*a*)] of three resonances at δ 196, 233 and 246 of intensity 2:1:1, respectively, which are assigned to terminal, edge- and face-bridging carbonyls, on the basis of their relative intensities and chemical shift values. On increasing the ^{13}CO enrichment to *ca.* 50% the two resonances at lower field, attributable to bridging carbonyls, become non-binomial triplets, as a result of coupling to each other ($^2J_{C-C}$ = 22.3 Hz). The reason for this coupling can be understood from Fig. 1: around each capping ruthenium atom, the edge- and face-bridging carbonyls are almost *trans* to each other, displaying an average angle μ-CO–Ru–μ_3-CO of 163.6°.

The sharpness of the peaks shows that the molecule is not

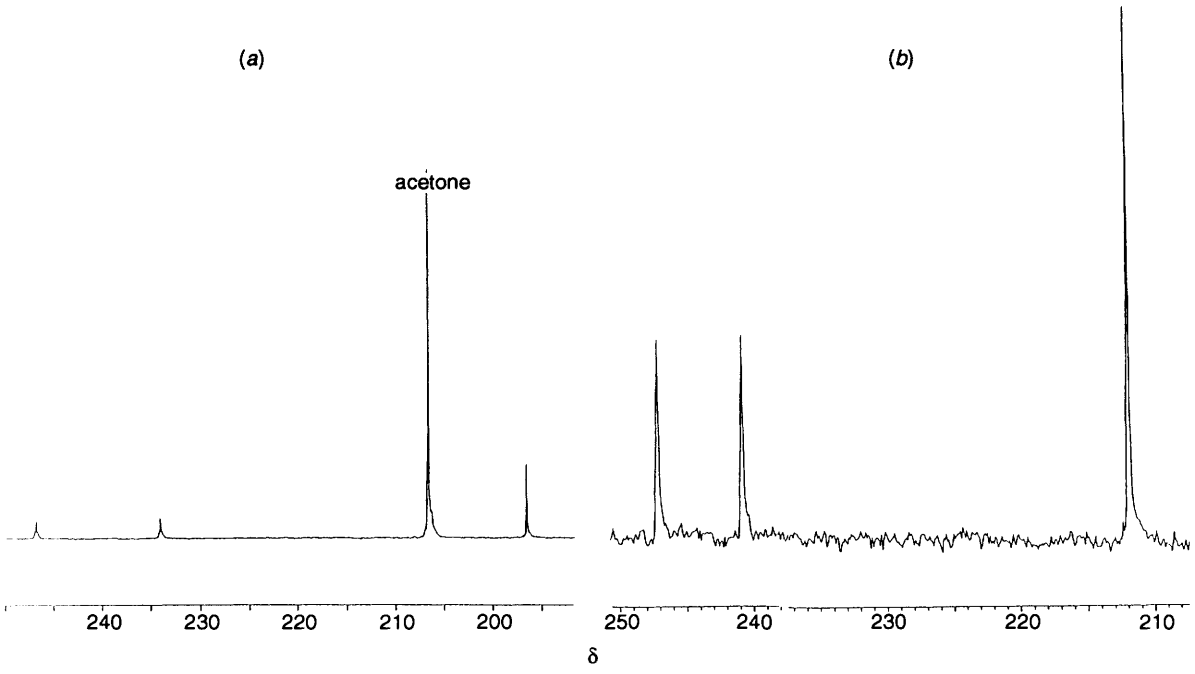

Fig. 5 The ^{13}CO NMR spectra in acetone, at 25 °C of (*a*) $[Pd_6Ru_6(CO)_{24}]^{2-}$ and (*b*) $[Fe_6Pd_6H(CO)_{24}]^{3-}$

fluxional, on the NMR time-scale, and the structure in the solid state and in solution appears to be the same despite the lack of a band in the solution IR spectrum which can be obviously attributed to the μ_3-CO.

$[Fe_6Pd_6H(CO)_{24}]^{3-}$. The ^{13}CO NMR spectrum of $[Fe_6Pd_6H(CO)_{24}]^{3-}$ (*ca.* 30% ^{13}CO), in acetone at 25 °C, consists of three resonances at δ 211, 241 and 248, of intensity 2:1:1 [Fig. 5(*b*)], similar to that found for $[Pd_6Ru_6(CO)_{24}]^{2-}$. The resonances of complex **2** are expected at lower fields than those found for **1** as a result of the increased negative charge and of the low-field shift of the carbonyl groups attached to lighter metals;[14] however these effects are remarkable for the terminal ligands, and very small for the palladium-bound bridging carbonyls.

Conclusion

Both the solid-state and solution structures of $[Pd_6Ru_6(CO)_{24}]^{2}$ and $[Fe_6Pd_6H(CO)_{24}]^{3-}$ are shown to be the same despite having different numbers of cluster valence electrons: 158 and 160, respectively. The electrochemical results show that $[Fe_6Pd_6H(CO)_{24}]^{3-}$ exhibits a higher redox flexibility than does $[Pd_6Ru_6(CO)_{24}]^{2-}$ and although the two clusters are able to assume the same number of cluster valence electrons {162 in both $[Pd_6Ru_6(CO)_{24}]^{6-}$ and $[Fe_6Pd_6H(CO)_{24}]^{5-}$, which can be electrochemically generated}, electrochemical measurements suggest that the pathways of these electron transfers are significantly different from each other for the ruthenium– and iron–palladium clusters, thus reflecting a different ordering level of the relevant molecular orbitals.

Experimental

All solvents were purified and dried by conventional methods and stored under nitrogen. All reactions were carried out under an oxygen-free nitrogen atmosphere using the Schlenk-tube technique.[15] The complexes $[Ru_3(CO)_{12}]$,[16] $[NEt_4][Ru_3H(CO)_{11}]$,[17] $[Pd(NCPh)_2Cl_2]$,[18] $[Fe(C_5H_5)_2]PF_6$[19] and $[NMe_3(CH_2Ph)]_3[Fe_6Pd_6H(CO)_{24}]$[5] were prepared by published methods. Infrared spectra were recorded on a Perkin-Elmer 781 grating spectrophotometer using calcium fluoride cells previously purged with N_2, NMR solution spectra on a Bruker AMX ACC spectrometer using CD_2Cl_2 sealed in a coaxial tube as external reference.

Materials and apparatus for electrochemistry and coupled EPR measurements have been described elsewhere.[20] All the potentials are referenced to the saturated calomel electrode (SCE). Under the present experimental conditions the one-electron oxidation of ferrocene occurs at +0.46 and +0.54 V in acetone and tetrahydrofuran solution, respectively. The paramagnetic species was electrogenerated at −20 °C. The external magnetic field H_0 for EPR measurements was calibrated by using a diphenylpicrylhydrazyl (dpph) powder sample (g_{dpph} = 2.0036).

Synthesis of $[NEt_4]_2[Pd_6Ru_6(CO)_{24}]$ **1**.—The compounds $[Ru_3(CO)_{12}]$ (0.150 g, 0.235 mmol) and $NaBH_4$ (0.050 g, 1.32 mmol) were dissolved in thf (15 cm^3), stirred (2 h) and filtered, followed by removal of thf under reduced pressure. The resulting crude product $Na[Ru_3H(CO)_{11}]$ was dissolved in methanol (10 cm^3) and the dark red solution cooled to −78 °C. The complex $[Pd(NCPh)_2Cl_2]$ (0.108 g, 0.281 mmol) was added while stirring and the mixture allowed to warm to room temperature. After 30 min the solution was filtered and the filtrate slightly concentrated under reduced pressure. Solid $[NEt_4]Br$ (0.5 g) was added, inducing partial precipitation of $[NEt_4]_2[Pd_6Ru_6(CO)_{24}]$; propan-2-ol (40 cm^3) was added to complete the precipitation. The solid $[NEt_4]_2[Pd_6Ru_6(CO)_{24}]$ was filtered off, washed with propan-2-ol (2 × 5 cm^3) and dried under vacuum, yield 0.060 g (58.5%). The sample is sufficiently pure for most synthetic purposes, as confirmed by satisfactory elemental analyses (Found: C, 21.65; H, 1.95; N, 1.20. $C_{40}H_{40}N_2O_{24}Pd_6Ru_6$ requires C, 22.05; H, 1.85; N, 1.30%).

Crystals of $[NEt_4]_2[Pd_6Ru_6(CO)_{24}]$ were grown by the slow-diffusion technique, dissolving the sample in thf or MeCN followed by layering with cyclohexane or diisopropyl ether, respectively.

Oxidation of $[Pd_6Ru_6(CO)_{24}]^{2-}$.—Complex **1** (0.100 g, 0.046 mmol) was dissolved in thf (10 cm^3) and solid $[Fe(C_5H_5)_2]PF_6$ added until the IR spectrum of the solution showed complete conversion into the oxidised product. Any attempt to grow crystals of the oxidised product by layering the thf solution with cyclohexane resulted in decomposition, with formation of black, insoluble material and the starting cluster $[NEt_4]_2[Pd_6Ru_6(CO)_{24}]$.

Table 5 Crystallographic data

Compound	$[NEt_4]_2[Pd_6Ru_6(CO)_{24}]$
Formula	$C_{40}H_{40}N_2O_{24}Pd_6Ru_6$
M	2177.6
Crystal system	Triclinic
Space group	$P\bar{1}$
a/Å	11.514(5)
b/Å	11.602(5)
c/Å	11.933(5)
α/°	73.01(3)
β/°	78.25(3)
γ/°	65.26(4)
U/Å^3	1379(1)
Z	1
$F(000)$	1026
D_c/g cm^{-3}	2.623
Crystal dimensions/mm	0.17 × 0.04 × 0.38
μ(Mo-Kα)/cm^{-1}	35.2
Minimum transmission factor	0.77
Scan mode	ω
ω-Scan width/°	1.6 + 0.35 tan θ
θ range/°	3–27
Reciprocal space explored	$+h, \pm k, \pm l$
Measured reflections	5968
Unique observed reflections [$I > 3\sigma(I)$]	4129
Final R and R' indices[a]	0.024, 0.026
No. of variables	352
Goodness of fit[b]	1.08

[a] $R = [\Sigma(F_o - k\|F_c\|)/\Sigma F_o]$, $R' = [\Sigma w(F_o - k\|F_c\|)^2/\Sigma w F_o^2]^{\frac{1}{2}}$. [b] $[\Sigma w(F_o - k\|F_c\|)^2/(N_o - N_v)]^{\frac{1}{2}}$ where $w = 1/[\sigma(F_o)]^2$, $\sigma(F_o) = [\sigma^2(I) + (0.025I)^2]^{\frac{1}{2}}/2F_oL_p$, N_o is the number of observations and N_v the number of variables.

Enrichment of $[Pd_6Ru_6(CO)_{24}]^{2-}$ **1** *and* $[Fe_6Pd_6H(CO)_{24}]^{3-}$ **2**.—Complex **1** is stable under CO and can be enriched in 12 h by direct exchange with ^{13}CO. The gas was handled using standard vacuum-line techniques. Enriched samples of **2** were obtained from the ^{13}CO-enriched starting material $[Fe_4(CO)_{13}]^{2-}$.[5]

X-Ray Data Collection and Structural Determination.—Crystal data and other experimental details are summarized in Table 5.

The diffraction experiment was carried out on an Enraf–Nonius CAD-4 diffractometer at room temperature using Mo-Kα radiation (λ = 0.710 73 Å) with a graphite crystal monochromator in the incident beam. The calculations were performed on a PDP11/73 computer using the SDP structure determination package[21] and the physical constants tabulated therein. Cell parameters were obtained from the accurate centring of 25 random reflections in the range θ 9–12°. A periodic monitoring of the intensities of three standard reflections did not show any crystal decay during data collection. The diffracted intensities were corrected for Lorentz, polarization and absorption effects (empirical correction).[22] Scattering factors and anomalous dispersion corrections were taken from ref. 23. The structure was solved by direct methods (MULTAN)[24] and refined by full-matrix least squares, minimizing the function $\Sigma w(F_o - k|F_c|)^2$. Anisotropic thermal factors were refined for all the non-hydrogen atoms. The hydrogen atoms were placed in their ideal positions (tetrahedral staggered conformation, C–H 0.95 Å, B = 5.5 Å^2). The final Fourier map showed maximum residuals of 0.50(10) e Å^{-3} at 0.95 Å from Ru(5) and 0.44(10) e Å^{-3} at 0.94 Å from Ru(4).

Additional material available from the Cambridge Crystallographic Data Centre comprises H-atom coordinates, thermal parameters and remaining bond lengths and angles.

Acknowledgements

We thank G. Longoni (Bologna, Italy) for helpful suggestions and discussion of results and the EEC [contract no. ST2J-0479-C(A)] for financial support.

References

1 E. Sappa, A. Tiripicchio and P. Braunstein, *Coord. Chem. Rev.*, 1985, **65**, 219; L. J. Farrugia, *Adv. Organomet. Chem.*, 1990, **31**, 301.
2 P. Zanello, *Struct. Bonding (Berlin)*, 1992, **79**, 101.
3 T. Chihara, R. Komoko, K. Kobayashi, H. Yamazaki and Y. Matsuura, *Inorg. Chem.*, 1989, **28**, 964; P. J. Bailey, M. A. Beswick, B. F. G. Johnson, J. Lewis, P. R. Raithby and M. C. Ramirez de Arellano, *J. Chem. Soc., Dalton Trans.*, 1992, 3159 and refs. therein.
4 K. C. Kharas and L. F. Dahl, *Adv. Chem. Phys.*, 1988, **70**, 1.
5 G. Longoni, M. Manassero and M. Sansoni, *J. Am. Chem. Soc.*, 1980, **102**, 3242.
6 G. Longoni, M. Manassero and M. Sansoni, *J. Am. Chem. Soc.*, 1980, **102**, 7973.
7 G. K. Johnson, ORTEP, Report ORNL-5138, Oak Ridge National Laboratory, Oak Ridge, TN, 1976.
8 B. K. Teo and N. J. A. Sloane, *Inorg. Chem.*, 1985, **24**, 4545.
9 D. M. P. Mingos, *Acc. Chem. Res.*, 1984, **17**, 311; D. M. P. Mingos and D. J. Wales, in *Introduction to Cluster Chemistry*, Prentice-Hall, Englewood Cliffs, NJ, 1990.
10 E. R. Brown and J. R. Sandifer, in *Physical Methods of Chemistry. Electrochemical Methods*. eds. A. Weissberger and B. W. Rossiter, Wiley-Interscience, New York, vol. 2, 1986.
11 P. Zanello, in *Stereochemistry of Organometallic and Inorganic Compounds*, ed. P. Zanello, Elsevier, Amsterdam, 1994, vol. 5, pp. 163–408.
12 J. P. Lozos, B. M. Hoffman and C. G. Franz, Quantum Chemistry Program Exchange, Program no. 265, Northwestern University, Evanston, IL, 1974.
13 C. T. Poole, jun. and H. A. Farach, in *Relaxation in Magnetic Resonance*, Academic Press, New York, 1971, p. 67.
14 B. E. Mann and B. E. Taylor, *^{13}C NMR data for Organometallic Compounds*, Academic Press, London, 1981, pp. 151–182.
15 D. F. Shriver and M. A. Drezdzon, *The Manipulation of Air-sensitive Compounds*, Wiley, New York, 2nd edn., 1986.
16 M. I. Bruce, C. M. Jensen and N. L. Jones, *Inorg. Synth.*, 1990, **28**, 217.
17 B. F. G. Johnson, J. Lewis, P. R. Raithby and G. Süss, *J. Chem. Soc., Dalton Trans.*, 1979, 1356.
18 G. K. Anderson and M. Lin, *Inorg. Synth.*, 1990, **28**, 60.
19 D. M. Duggan and D. N. Hendrickson, *Inorg. Chem.*, 1975, **14**, 955.
20 C. Bianchini, F. Laschi, D. Masi, F. M. Ottaviani, A. Pastor, M. Peruzzini, P. Zanello and F. Zanobini, *J. Am. Chem. Soc.*, 1993, **115**, 2723.
21 B. A. Frenz and Associates, SDP Plus Version 1.0, Enraf–Nonius, Delft, 1980.
22 A. C. T. North, D. C. Phillips and F. S. Mathews, *Acta Crystallogr., Sect. A*, 1968, **24**, 351.
23 D. T. Cromer and J. T. Waber, *International Tables for X-Ray Crystallography*, Kynoch Press, Birmingham, 1974, vol. 4.
24 P. Main, S. J. Fiske, S. E. Hill, L. Lessinger, G. Germain, J. P. Declercq and M. M. Wolfson, MULTAN 80, A system of computer programs for the automatic solution of crystal structures from X-ray diffraction data, Universities of York and Louvain, 1980.

Received 10*th May* 1994; *Paper* 4/02780I